

## **Decreased mitochondrial DNA content drives OXPHOS dysregulation in chromophobe renal cell carcinoma**

Yi Xiao<sup>1,2</sup>, Rosanna Clima<sup>3,4</sup>, Jonas Busch<sup>5</sup>, Anja Rabien<sup>5,6</sup>, Ergin Kilic<sup>7,8</sup>, Sonia L. Villegas<sup>8</sup>, Bernd Timmermann<sup>1</sup>, Marcella Attimonelli<sup>3</sup>, Klaus Jung<sup>5,6</sup>, and David Meierhofer<sup>1,\*</sup>

### Author Affiliations

<sup>1</sup>Max Planck Institute for Molecular Genetics, Ihnestrasse 63-73, 14195 Berlin, Germany

<sup>2</sup>Department of Biology, Chemistry, Pharmacy, Freie Universität Berlin, Arnimallee 22, 14195 Berlin, Germany

<sup>3</sup>Department of Biosciences, Biotechnology, and Biopharmaceutics, University of Bari, Via E.Orabona, 470126 Bari, Italy

<sup>4</sup>Department of Medical and Surgical Sciences-DIMEC, Medical Genetics Unit, University of Bologna, Bologna, Italy

<sup>5</sup>Department of Urology, Charité – Universitätsmedizin Berlin, corporate member of Freie Universität Berlin, Humboldt-Universität zu Berlin, and Berlin Institute of Health, 10117 Berlin, Germany

<sup>6</sup>Berlin Institute for Urologic Research, Charitéplatz 1, 10117 Berlin, Germany

<sup>7</sup>Institut für Pathologie am Klinikum Leverkusen, Am Gesundheitspark 11, 51375 Leverkusen, Germany

<sup>8</sup>Institute of Pathology, Charité – Universitätsmedizin Berlin, corporate member of Freie Universität Berlin, Humboldt-Universität zu Berlin, and Berlin Institute of Health, 10117 Berlin, Germany

**Running title:** OXPHOS dysregulation in chromophobe renal cell carcinoma

**Key words:** Chromophobe renal cell carcinoma (chRCC); Renal oncocytoma (RO); oxidative phosphorylation (OXPHOS); mitochondrial DNA content; glutathione metabolism.

\*Correspondence should be addressed to: David Meierhofer, Ihnestrasse 63-73, 14195 Berlin, Germany. Phone: +4930-8413-1567; FAX: +4930-8413-1960; email: meierhof@molgen.mpg.de.

The authors declare no potential conflicts of interest.

## **Abstract**

Chromophobe renal cell carcinoma (chRCC) and renal oncocytoma (RO) are closely related, rare kidney tumors. Mutations in complex I (CI)-encoding genes play an important role in dysfunction of the oxidative phosphorylation (OXPHOS) system in RO but are less frequently observed in chRCC. As such, the relevance of OXPHOS status and role of CI mutations in chRCC remain unknown. To address this issue, we performed proteome and metabolome profiling as well as mitochondrial whole-exome sequencing to detect mitochondrial alterations in chRCC tissue specimens. Multi-omic analysis revealed downregulation of electron transport chain (ETC) components in chRCC that differed from the expression profile in RO. A decrease in mitochondrial (mt)DNA content, rather than CI mutations, was the main cause for reduced OXPHOS in chRCC. There was a negative correlation between protein and transcript levels of nuclear DNA- but not mtDNA-encoded ETC complex subunits in chRCC. In addition, the reactive oxygen species scavenger glutathione (GSH) was upregulated in chRCC due to decreased expression of proteins involved in GSH degradation. These results demonstrate that distinct mechanisms of OXPHOS exist in chRCC and RO and that expression levels of ETC complex subunits can serve as a diagnostic marker for this rare malignancy.

**Significance:** Findings establish potential diagnostic markers to distinguish malignant chRCC from its highly similar but benign counterpart, renal oncocytoma.

## Introduction

Chromophobe renal cell carcinoma (chRCC) and renal oncocytoma (RO) originate from intercalated cells of the collecting duct, with each accounting for approximately 5% of all renal neoplasms (1,2). The World Health Organization (WHO) chRCC classification guidelines define a classic and an eosinophilic variant (1). Classic chRCC (about 75-80% of chRCC) consist of large cells with reticular cytoplasm and prominent cell membranes (pale) cells that are characterized by numerous cytoplasmic microvesicles, which is probably related to defective mitochondrial development, whereas mitochondria are abundant in the eosinophilic phenotype (3-6). The characteristic genetic feature of chRCC is monosomy of chromosomes 1, 2, 6, 10, 13, 17, and often 21 (7-9). Although the typical mutations in tumor protein 53 (*TP53*; 32%) and phosphatase and tensin homolog (*PTEN*; 9%) genes have been reported (7,10,11), chRCC has a low mutational burden overall; there are no clear driver mutations in >50% of chRCC cases (10,11). This is in contrast to clear cell (cc)RCC in which the frequency of the Von Hippel-Lindau (*VHL*) gene mutation is >80% (12).

RO is classified as a benign renal epithelial neoplasm (13,14) that is usually treatable by nephrectomy. The main molecular hallmark of RO is the marked reduction or complete loss of complex I (CI) enzyme activity in the electron transport chain (ETC) (15,16). This is primarily caused by mutations in mitochondrial (mt)DNA and especially, but not exclusively, in genes encoding CI subunits (15,17). Most of the mtDNA mutations are well above the threshold for a pathogenic phenotypic effect resulting from high heteroplasmic loads (15,17), and inhibit tumor growth through adverse effects on respiratory complex assembly (18,19). Thus, mtDNA mutations are thought to be the main cause of the indolent, low-proliferating, non-invasive behavior of RO and are driving the cancer phenotype (17,20,21).

ChRCC is considered as the malignant counterpart to RO (21) with similar origin, gene expression patterns, and mitochondrial pathology, making them difficult to distinguish histologically (2,10,21). The 2 tumor types have distinct mtDNA mutation profiles (18,19). In

contrast to RO, only 13% of chRCC cases harbor CI mutations, with a heteroplasmy rate >50% (22). Transcriptome analyses have shown that chRCC cases with mutations in CI subunit-encoding genes did not have RNA expression patterns associated with loss of oxidative phosphorylation (OXPHOS) (22,23), contrary to expectation (24). This suggests possible alternative roles for CI mutations in OXPHOS or, as-yet unknown, compensatory mechanisms leading to increased transcript levels of OXPHOS-related factors. It was recently reported that chRCC and RO have elevated levels of GSH (25-29), which is a novel hallmark of all RCCs and a potential therapeutic target (30). Enhanced GSH biosynthesis in RO is presumed to be an adaptive event resulting from loss-of-function mutations in CI subunits (25,26). However, given the low frequency of CI mutations in chRCC (22), it is likely that the elevated GSH level is the result of an alternative mechanism.

Here we demonstrate that protein levels of ETC complex subunits were decreased whereas global mitochondrial mass was unchanged in chRCC compared to healthy kidney tissue. This is in contrast to RO, in which there was a general increase in mitochondrial mass but not in CI subunit expression. There was a negative correlation between protein and mRNA levels of ETC complex subunits in chRCC, and a reduction in mtDNA content rather than CI mutations was found to be responsible for the decrease in OXPHOS. Interestingly, GSH levels increased with mtDNA depletion. These features may serve as markers for distinguishing between these 2 closely related tumor types.

## **Materials and Methods**

### **Sample Acquisition and Verification**

Nine pairs of chRCC and adjacent healthy kidney tissue derived from nephrectomies at the Charité – Universitätsmedizin Berlin were collected in liquid nitrogen within 30 minutes after surgery and preserved at -80°C. The clinical characteristics of the tumors are reported in Table

S1. From the collected tissue samples, histologic sections were stained with hematoxylin and eosin. The diagnosis of chRCC and the corresponding matched tumor-free kidney tissue was done according to the WHO classification criteria. Only cases with a clear diagnosis of chRCC were considered for the study. The typical genetic feature of chRCC, the monosomy of chromosomes 1, 2, 6, 10, 13, 17, and 21, was confirmed in all cases by analyzing the chromosome copy number variation based on the whole-exome sequencing data (Figure S1). The study was approved by the institutional Ethics Committee (no. EA1/134/12) and was carried out in accordance with the Declaration of Helsinki. All participants gave written informed consent.

### **Proteomic Analysis**

The tissue samples for proteomics were processed with iST 96X kits following the manufacturer's protocol (iST sample preparation kit 96X, PreOmics, Martinsried, Germany). Briefly, tissues were homogenized under denaturing conditions with a FastPrep (three times for 60 s,  $6.5 \text{ m} \times \text{s}^{-1}$ ), followed by boiling at  $95^\circ\text{C}$  for 10 min. The lysates containing  $40 \mu\text{g}$  protein were then digested by trypsin and Lys-C protease mixture at  $37^\circ\text{C}$  overnight. Subsequently, the peptides were purified with the cartridge and each sample was further separated using three fractions according to (31). A total of  $10 \mu\text{g}$  of each fraction was analyzed by LC-MS for proteome profiling. All fractions were allocated to the corresponding replicate and analyzed jointly by the software tool MaxQuant (32).

LC-MS/MS was carried out by nanoflow reverse-phase liquid chromatography (Dionex Ultimate 3000, Thermo Scientific, Waltham, MA) coupled online to a Q-Exactive HF Orbitrap mass spectrometer (Thermo Scientific, Waltham, MA). Briefly, the LC separation was performed using a PicoFrit analytical column ( $75 \mu\text{m}$  ID  $\times$  55 cm long,  $15 \mu\text{m}$  Tip ID (New Objectives, Woburn, MA) in-house packed with  $3\text{-}\mu\text{m}$  C18 resin (Reprosil-AQ Pur, Dr. Maisch, Ammerbuch-

Entringen, Germany). Peptides were eluted using a gradient from 3.8 to 40% solvent B in solvent A over 120 min at 266 nL per minute flow rate. Solvent A was 0.1 % formic acid and solvent B was 79.9% acetonitrile, 20% H<sub>2</sub>O, 0.1% formic acid. Nanoelectrospray was generated by applying 3.5 kV. A cycle of one full Fourier transformation scan mass spectrum (300–1750 m/z, resolution of 60,000 at m/z 200, AGC target 1e<sup>6</sup>) was followed by 16 data-dependent MS/MS scans (resolution of 30,000, AGC target 5e<sup>5</sup>) with a normalized collision energy of 27 eV. In order to avoid repeated sequencing of the same peptides, a dynamic exclusion window of 30 sec was used. In addition, only peptide charge states between two to eight were sequenced.

Raw MS data were processed with MaxQuant software (v1.6.0.1) (32) and searched against the human proteome database UniProtKB with 70,941 entries, released in 01/2017. Parameters of MaxQuant database searching were: A false discovery rate (FDR) of 0.01 for proteins and peptides, a minimum peptide length of 7 amino acids, a mass tolerance of 4.5 ppm for precursor and 20 ppm for fragment ions were required. A maximum of two missed cleavages was allowed for the tryptic digest. Cysteine carbamidomethylation was set as a fixed modification, while N-terminal acetylation and methionine oxidation were set as variable modifications. MaxQuant processed output files can be found in Table S2, showing peptide and protein identification, accession numbers, % sequence coverage of the protein, q-values, and LFQ intensities. Contaminants, as well as proteins that were only identified by site modifications and proteins derived from the reversed part of the decoy database, were strictly excluded from further analysis.

### **Metabolite Profiling**

About 30 mg of nine unrelated and N<sub>2</sub> shock frozen chRCC and corresponding healthy kidney tissues were used for metabolite profiling. Metabolite extraction and tandem LC-MS measurements were done as previously reported by us (25). In brief, methyl-tert-butyl ester

(MTBE), methanol, ammonium acetate, and water were used for metabolite extraction. The subsequent separation was performed on an LC instrument (1290 series UHPLC; Agilent, Santa Clara, CA), online coupled to a triple quadrupole hybrid ion trap mass spectrometer QTrap 6500 (Sciex, Foster City, CA), as reported previously (33). Transition settings for multiple reaction monitoring (MRM) are provided in Table S3.

The metabolite identification was based on three levels: (i) the correct retention time, (ii) up to three MRM's and (iii) a matching MRM ion ratio of tuned pure metabolites as a reference (33). Relative quantification was performed using MultiQuant™ software v.2.1.1 (Sciex, Foster City, CA). The integration setting was a peak splitting factor of 2 and all peaks were reviewed manually. Only the average peak area of the first transition was used for calculations. Normalization was done according to used amounts of tissues and subsequently by internal standards, as indicated in Table S3.

### **Determination of Free and Total GSH in Plasma and Urine**

The GSH level in plasma- (6 RO, 6 ccRCC, 12 pRCC, 6 chRCC, and 6 healthy) and urine specimens (8 RO, 20 ccRCC, 19 pRCC, 7 chRCC, and 20 healthy) was investigated to see if it can be used as a non-invasive metabolic marker. Free and total GSH were measured using a GSH fluorescent detection kit (cat.no. EIAGSHF) according to the manufacturer's protocol (Invitrogen, Carlsbad, CA).

### **Enzyme Activity Measurement**

Sample preparation to spectrophotometrically assay enzyme activity was done as reported previously (33). In brief, approximately 5 mg of the tumor and healthy kidney tissues were homogenized and centrifuged at 600 g at 4 °C for 10 min. The protein concentrations of supernatants were further determined with a BCA assay (Thermo Fisher, Germany). For

complex I, II, and V, 4  $\mu\text{g}$  protein of each sample were used for the enzymatic activity measurement; for complex III, and IV, 2  $\mu\text{g}$  protein was used. Rotenone (10  $\mu\text{M}$ ), malonic acid (5 mM), antimycin A (5  $\mu\text{g}/\text{ml}$ ), potassium cyanide (500  $\mu\text{M}$ ), and oligomycin (5  $\mu\text{g}/\text{ml}$ ) served as specific inhibitors for complex I to V, respectively.

### **Whole Exome Sequencing and Mitochondrial Bioinformatics Analysis**

DNA was isolated from the remaining pellets after metabolite extraction with a DNA purification kit according to the manufacturer's protocol (QIAamp DNA Mini Kit for Tissues, QIAGEN, Hilden, Germany). In brief, the pellets were lysed by proteinase K and the RNA was removed by RNase, the RNA-free genomic DNA was then purified and eluted on QIAamp Mini spin columns for library preparation. The library preparation was performed according to Agilent's SureSelect protocol (SureSelectXT Human All Exon V5, protocol version B4 August 2015) for Illumina paired-end sequencing, as reported previously (25). The fastq files were used as input for the MToolBox pipeline (34), in order to extract mitochondrial DNA sequences and quantify each variant allele heteroplasmy, as done previously (25). Copy number variation (CNV) was inferred and visualized with the CNVkit (35).

### **Analysis of TCGA RNA-seq Data**

TCGA (ID: KICH) RNA-seq data were obtained from UCSC Xena (36) (<https://xenabrowser.net/>). Accurate transcript quantification of chRCC (n=66) and controls (n=25) was based on the RNA-Seq by the Expectation Maximization method (37).

## **Cell Culture**

The recently established and chRCC-derived cell line UOK276 (38) was a kind gift from Prof. Marston Linehan (Center for Cancer Research at the National Cancer Institute, USA). The ccRCC derived cell line 786-O and the normal kidney cell line HK2 were obtained from ATCC. No mycoplasma testing were performed before the experiments. The three cell lines were cultivated in Dulbecco's modified Eagle medium (DMEM, Life Technologies, New York, NY) containing 4.5 g/L glucose, supplemented with 10% fetal bovine serum (FBS, Silantes, Munich, Germany) and 1% penicillin-streptomycin-neomycin (Invitrogen, Carlsbad, CA) at 37°C in a humidified atmosphere of 5% CO<sub>2</sub>.

The three types of cells were seeded into 6-well plates and the cell medium was supplemented with 100 ng/ml ethidium bromide (EtBr) and 50 µg/ml uridine to induce mtDNA depletion. On days 0, 2, 5, 8, 13, and 19, the cells were collected and frozen immediately at -80°C for the measurement of GSH, mtDNA, RNA and protein correlation.

## **Western blotting**

The proteins were extracted from the cells by using the TRIzol reagent (Sigma), and then resolved by SDS-PAGE. Separated proteins were transferred to polyvinylidene fluoride membranes and incubated with indicated primary antibodies diluted in TBST (20 mM Tris, 150 mM NaCl, and 0.1% Tween 20) supplemented with 5% bovine serum albumin (Sigma). Primary antibodies were detected with horseradish peroxidase-conjugated secondary antibodies followed by exposure to ECL reagents (Bio-Rad). The used primary antibodies and dilutions are as follows: Anti MT-ND5 (Thermo Fisher, PA5-39277, 1:500); anti NDUFS1 (Proteintech, 12444-1-AP, 1:1000); anti SDHB (Sigma, HPA002868, 1:500); anti UQCRC2 (Sigma, HPA007998, 1:250).

## Quantitative PCR

Total RNA and the genomic DNA were isolated using the TRIzol reagent (Sigma), and the QIAamp DNA micro kit (Qiagen) according to the manufactures' instruction, respectively. The quantitative PCR analysis was performed using GoTaq qPCR regents (Promega) mixed with indicated primers in a 7900 Real-Time PCR system (Applied Biosystems). Pre-designed primers were synthesized by Eurofins Genomics detecting the following transcripts: MT-ND5 (5'-CCGGAAGCCTATTCGCAGGA, 5'-ACAGCGAGGGCTGTGAGTTT), NDUFS1 (5'-TGCTGAAGCCCTGGTAGCTC, 5'-TGCCTCTTCCACACCAGCAA), SDHB (5'-GACGGGCTCTACGAGTGCAT, 5'-TGATGGTGTGGCAGCGGTAT), UQCRC2 (5'-AACCACCCATTTGCTGCGTC, 5'-TCCCTTGTTGCGGTCACACT), SLC1A4 (5'-AGCAGCCATCTTCCAGTGTGT, 5'-GGTCATGAGTAGGCAGCCCAA). The depletion of mtDNA in EtBr treated cells was verified by quantifying a 399-bp mtDNA product that spans the region of nt 3153 – nt 3551 (Primer: 5'-TTCACAAAGCGCCTTCCCCCGT, 5'-GCGATGGTGAGAGCTAAGGTCGGG) and a 238-bp nuclear DNA product that spans the region of exon 5 (nt 55953445 – nt 55953207) of the gene USMG5 (Primer: 5'-AGTGTCTTAAGAGTAAAGCTGGCCACA, 5'-TTGCCTTTGTTGCATTTTCTACAG).

## Experimental Design and Statistical Rationale, and Pathway Analyses

For proteome and metabolome data sets, a two-sample t-test was performed. Multiple test correction was done by Benjamini-Hochberg with an FDR of 0.05 by using Perseus (v1.6.0.2) (39). Significantly regulated proteins and metabolites were marked by a plus sign in the corresponding Tables S2 and S3. The Mann–Whitney *U* test was used to determine whether GSH levels from independent urine and plasma samples have the same distribution; the p-value significance cut-off was  $\leq 0.01$ .

For comprehensive proteome data analyses, gene set enrichment analysis (GSEA, v3.0) (40) was applied in order to see, if a *priori* defined sets of proteins show statistically significant, concordant differences between chRCC and kidney tissues. Only proteins with valid values in at least six of nine samples in at least one group with replacing missing values from the normal distribution for the other group were used (Table S2). GSEA default settings were applied, except that the minimum size exclusion was set to 10 and KEGG v6.2 was used as a gene set database. The cut-off for significantly regulated pathways was set to a p-value  $\leq 0.01$  and FDR  $\leq 0.05$ .

### **Data Availability**

The datasets generated in the current study are available as supplementary files and in the following repositories:

WES files can be accessed via <https://www.ncbi.nlm.nih.gov/sra> with the accession number: PRJNA413158. Proteomics raw data have been deposited to the ProteomeXchange Consortium via the Pride partner repository (41) with the dataset identifier PXD019123. Metabolomics data have been deposited in the publically available repository PeptideAtlas with the identifier PASS01250 and can be downloaded via <http://www.peptideatlas.org/PASS/PASS01250>.

### **Results**

#### **Proteomic Analysis Reveals OXPHOS Dysregulation in ChRCC**

The loss of CI and compensatory increases in the protein levels and enzymatic activity of the other ETC complexes are the primary molecular hallmarks of RO (15,16,25,26). To determine whether mitochondrial dysfunction is also present in chRCC, we carried out a proteomic analysis of 9 chRCC and adjacent normal kidney tissue samples (Table S1). There was a

general decrease in the expression of ETC complex subunits in chRCC relative to normal kidney tissue that predominantly affected CI (Fig. 1A), as determined with the t test with Benjamini-Hochberg correction (false discovery rate [FDR] < 0.05) (Table S2). The average log<sub>2</sub> fold change (chRCC vs kidney) was -1.79 for CI, -1.05 for CII, -0.91 for CIV, and -0.57 for CV, with no change observed for CIII (Fig. 1A). A comparison with RO proteome data (25) revealed that only CI subunits were downregulated in both tumors, whereas protein levels of the components of all other complexes were increased in RO and decreased in chRCC relative to normal tissue (Fig. 1A and B). It is worth noting that increased mitochondrial mass, a histological hallmark of RO, was consistently observed by allocation analysis of the proteome data, with mitochondrial proteins showing an obvious shift towards upregulation (Fig. 1C). This confirmed the strong reduction or complete loss of CI in RO (15,25), as the increased mitochondrial mass would be expected to reflect an increase in all mitochondrial proteins. However, allocation analysis of the chRCC proteome did not reveal any significant shifts in mitochondrial proteins (Fig. 1D), indicating that the decrease in OXPHOS in chRCC relative to normal kidney tissue does not result from a change in the amount of mitochondria.

A comparative proteome analysis of chRCC and RO revealed a marked reduction of CI in both tumor types, whereas other ETC complexes showed opposite trends in RO vs chRCC (upregulated and downregulated, respectively), suggesting that differences in OXPHOS are a potential marker for distinguishing between the two types of tumor.

### **ChRCC Exhibits a Discrepancy between mRNA and Protein Levels of ETC Complex Subunits**

In contrast to the decreased abundance of ETC complex proteins observed by proteome profiling, a transcriptome analysis of chRCC (Kidney Chromophobe dataset from The Cancer Genome Atlas [TCGA]) indicated that genes encoding ETC components were highly expressed (10,23). Gene Set Enrichment Analysis (GSEA) (40) of all quantified proteins showed a negative

enrichment score (-0.36) for the Kyoto Encyclopedia of Genes and Genomes pathway “oxidative phosphorylation” (Fig. 2A) but a positive score (0.47) for the transcriptome data (Fig. 2B). We therefore performed a correlation analysis of proteome and transcriptome data and found a high overall correlation between protein and mRNA levels ( $r=0.671$ ) similar to the value for all compounds of mitochondria ( $r=0.712$ ; Fig. 2C). However, the protein abundance of individual ETC complex subunits showed a low correlation with the corresponding transcript ( $r=0.196$ ).

To clarify the biological significance of this inverse and ETC specific regulation of the proteome and transcriptome, we compared the enzyme activity of all ETC complexes between chRCC and adjacent healthy kidney tissue samples and found a significant reduction in the activities of CI, CII, CIV, and CV, but no change in that of CIII in chRCC (Fig. 2D–H), which was consistent with the observed trend in protein levels (Fig. 1A).

### **GSH Level is Increased Whereas Expression of GSH-degrading Enzymes Is Decreased in ChRCC**

Reactive oxygen species (ROS) are produced by the ETC, primarily by CI and CIII (42,43). The levels of GSH, the major intracellular ROS scavenger, as well as its related metabolites are elevated in RO as an adaptive response to CI deficiency (25,26). Here we found that the top three metabolites with higher levels in chRCC compared with normal kidney tissue were all related to GSH metabolism, i.e., GSH (115 fold), glutathione disulfide (GSSG, 54 fold), and gamma-glutamylcysteine (15 fold) (Fig. 3A–C and Table S3). GSH/GSSG ratio, an indicator of cellular oxidative stress status (44), was increased in all chRCC samples except the Case 4 sample (Fig. 3D), implying a general reduction in oxidative stress in chRCC resulting from the  $\geq 100$ -fold higher GSH and GSSG levels compared to a normal kidney. Contrary to the increased levels of GSH-related metabolites, the GSH metabolism pathway was underrepresented ( $P \leq 0.005$ ) in the chRCC proteome GSEA (Table S2). This was mainly due

to downregulation (42-fold lower on average) of GSH-degrading and -conjugating enzymes such as gamma-glutamyltransferase (GGT)1, GGT5, glutathione S-transferase mu (GSTM)2, GSTM3, GST alpha 1 (GSTA1), and aminopeptidase N (ANPEP), as well as GSH peroxidase (GPX)3, which catalyzes the reduction of hydrogen peroxide (Fig. 3E). However, expression of glutathione synthetase and glutamate-cysteine ligase (GSS and GCLC, 2 key enzymes involved in GSH synthesis) and the other GSH-related enzymes, GPX1 and GPX4, the GSH S-transferases GST omega 1 (GSTO1) and GST pi 1 (GSTP1), and GSH reductase (GSR) were not significantly altered (Fig. 3E). Thus, the elevated levels of GSH-related metabolites in chRCC are attributable to a decreased abundance of proteins involved in GSH degradation, and not to an increase in GSH synthesis.

We analyzed free and total GSH levels in the plasma and urine of ccRCC, papillary (p)RCC, chRCC, and RO patients vs controls to determine whether GSH can serve as a non-invasive diagnostic marker. The results showed that free (Fig. S2A and B) and total (Fig. S2C and D) GSH levels were similar across tumor types. Thus, urine or plasma GSH levels are not a useful metabolic marker for distinguishing between renal tumor types and healthy individuals.

### **Decreased mtDNA Content and Mutations Lead to OXPHOS Dysfunction in chRCC**

To investigate whether mtDNA mutations are the main cause of OXPHOS dysfunction in chRCC, as in RO (15-17,25,26), we examined assembled mitochondrial whole-exome sequencing (WES) reads to identify somatic and germline mtDNA mutations in chRCC by pairwise comparisons between tumor and healthy tissues. We found adequate coverage (>99.9%) and quality for reliable mtDNA reconstruction and variant calling (Table S4). Neither the common deletion (mDNA<sup>4977</sup>), a 4977 bp deletion of mtDNA that specifically disrupts CI, CIV, and CV on the ETC, causes a wide spectrum of clinical manifestations (45), and is suspected to be associated with carcinogenesis (46), nor any other mtDNA deletions were detected in our chRCC cohort. Five somatic non-synonymous events were identified with a high

disease score (>0.7) that are potentially pathogenic (Fig. 4A and Table S4): 4 involved CI genes from 4 cases and 1 involved CIV genes. The chRCC specimen for Case 4—the only sample with a GSH/GSSG ratio lower than that of adjacent healthy tissue—harbored a somatic mutation in the mitochondria-encoded NADH-ubiquinone oxidoreductase chain 5 protein gene (*MT-ND5*; >60% heteroplasmy). The very low rate of heteroplasmy for the other events, i.e., 2 events <30%, 2 at ~5%, and no non-synonymous CI mutations in the remaining chRCC cases (Fig. 4A and Table S4), suggests that mechanisms other than loss-of-function mutations in CI lead to OXPHOS dysfunction and increase GSH levels in some chRCC cases.

$\rho^0$  cells are devoid of mtDNA and show drastic reduction of all ETC proteins (47). As a lower mtDNA copy number has been reported in chRCC (48), we speculated that the decreased levels of ETC complex subunits could be explained by a fewer number of copies of mtDNA. To evaluate mtDNA copy number in chRCC, we compared mtDNA reads between chRCC and healthy kidney tissue, as read depth in a specific region of the genome is roughly proportional to DNA copy number in that region. The mtDNA read depth was decreased 3 fold in chRCC relative to normal tissue (Fig. 4B), indicating a lower mtDNA content.

### **Low mtDNA Content Causes Downregulation of ETC Complex Subunits and Elevation of GSH Levels**

To investigate the influence of mtDNA content on protein and transcript levels of ETC complex subunits and GSH levels, UOK276 (a chRCC cell line) (38), was chronically exposed to a low concentration of ethidium bromide (EtBr) for 19 days to deplete mtDNA (49). Samples collected on days 0, 2, 5, 8, 13, and 19 for analysis showed that mtDNA content decreased within 5 days and reached  $\rho^0$  status (complete mtDNA depletion) after 13 days (Fig. 5A). The protein levels of 4 ETC complex subunits, including those encoded by mtDNA (*MT-ND5* [CI]) and nuclear DNA (NADH:ubiquinone oxidoreductase core subunit [*NDUFS1*] [CI], succinate dehydrogenase complex iron sulfur subunit [*SDH]B* [CII], and ubiquinol-cytochrome C reductase core protein

[UQCRC]2 [CIII]), were analyzed by Western blotting. All subunits showed a time-dependent decrease in expression and were almost undetectable after 13 days (Fig. 5B), implying a direct link between mtDNA depletion and a reduction in ETC proteins.

We next performed metabolome profiling to determine whether GSH levels correlated with mtDNA depletion in  $\rho^0$  cells and found that they increased during the process of mtDNA depletion, reaching a plateau on day 13 (Fig. 5C). Interestingly, there were 2 distinct mRNA expression profiles for the 4 ETC complex subunits: nuclear DNA-encoded transcripts decreased until day 8 (NDUFS1) or day 13 (SDHB and UQCRC2), before increasing (Fig. 5D). The mRNA levels were mostly unrelated to those of the corresponding protein (Fig. 5B). A notable exception was the transcript level of the mtDNA-encoded MT-ND5, which decreased after just 2 days and did not recover (Fig. 5D), closely mirroring protein expression (Fig. 5B). The same EtBr experiments were performed in the ccRCC cell line 786-O (harboring the Von Hippel-Lindau gene mutation) and normal human kidney cell line (HK-2) to see whether the decrease of mtDNA content and OXPHOS dysfunction is chRCC specific. Similar results were found in these two cell lines compared with that in UOK276 cells (Fig. S3A-D). Taken together, these results indicate that the decrease in mtDNA content is the main cause of OXPHOS dysfunction in chRCC and leads to an elevation in GSH levels.

## **Discussion**

Although chRCC was identified 30 years ago as a type of kidney cancer (50), it is not well understood because of its rarity. Two recent studies comprising around 100 cases investigated the genetic causes of chRCC but failed to identify obvious driver mutations in >50% of cases (10,23). In contrast, mutations in CI genes and mitochondrial abnormalities are frequently observed in RO. To investigate the characteristics of mitochondria in chRCC and their role in disease progression, we used a combination of proteomic, transcriptomic (TCGA), and metabolomic approaches, and performed mitochondrial WES to elucidate the mtDNA mutation

landscape and identify differences in mitochondrial function between chRCC and healthy adjacent kidney tissue. Our results showed that a decrease in mtDNA content, and not mutational load, was the main cause of the observed decreases in the levels and activity of nearly all ETC complex subunits (except for CIII), which increased GSH levels and resulted in a discrepancy between mRNA and protein levels of these subunits.

As in many cancer types, glycolytic metabolism is enhanced in chRCC (28). In company with the downregulation of OXPHOS found in this study, we propose that chRCC features the typical “Warburg effect”. We previously reported that the activity of all mitochondrial enzymes was reduced in ccRCC and pRCC (48). This is in contrast to the benign RO, in which only CI subunits show reduced expression and activity, which are increased for all other complexes (25).

The metabolites showing the greatest increase in chRCC relative to healthy adjacent kidney tissue were those involved in GSH metabolism (GSH, GSSG, and gamma-glutamylcysteine), which is consistent with findings for chRCC (27,28), pRCC (51), RO (25,26), and ccRCC (52,53). As GSH is an ROS scavenger (54), the increased GSH levels and GSH/GSSG ratio in chRCC may be a strategy for the tumor to overcome ROS stress originating from dysregulated OXPHOS. As in RO, the abundance of enzymes involved in GSH synthesis was unchanged in chRCC whereas the level of enzymes involved in GSH degradation was reduced, resulting in high levels of GSH in tumor cells and a microenvironment with a low oxidative stress burden.

The opposite trends in transcript and protein levels of ETC components observed in our chRCC cohort has also been reported in RO (25). The negative correlation suggests that the pathogenic mechanisms of RCC can only be understood by evaluating different levels of molecular information. For example, the enzymatic activity of ETC complex subunits in chRCC and RO (15) corresponds to the abundance of the proteins and not gene expression. A study of mtDNA-depleted  $\rho^0$  cells showed that the levels of all ETC components were significantly

reduced because complex assembly is not possible without the core mtDNA-encoded subunits (47). Thus, the inverse relationship between transcript and protein levels in chRCC was mainly due to reduced mtDNA content. This was confirmed by monitoring mtDNA depletion and the abundance of ETC complex subunits over time in a chRCC cell line. All proteins involved in OXPHOS were decreased in parallel with mtDNA content, but there was a discrepancy between mtDNA- and nuclear DNA-encoded ETC complex subunits: the former almost completely disappeared whereas the latter remained stable when cells reached  $\rho^0$  status. In addition, GSH levels were negatively correlated with mtDNA content, indicating that defective respiration might cause ROS stress, which is compensated for by an increase in the level of GSH, the main ROS scavenger. Another possibility is that the dysfunctional OXPHOS impairs the turnover of NADH and NADPH and thus keeps reduced GSH in chRCC at a higher level.

The mitochondrial genome in RO and thyroid cancers have a high mutational burden (15,17,55). Although we identified multiple potentially pathogenic mtDNA mutations with mostly low heteroplasmy loads (except Case 4, which harbored a mutated *MT-ND5* gene with >60% heteroplasmy), these low heteroplasmic mtDNA mutation rates are unlikely to influence chRCC phenotype as the cases did not show differential regulation of OXPHOS and shared the same overall proteome profile. Although all chRCC cases had similarly high levels of GSH and related metabolites, Case 4 showed a decreased GSH/GSSG ratio in chRCC relative to normal kidney tissue, unlike the other cases. This indicates that oxidative stress was increased by the mutation in the *MT-ND5* gene, possibly through increased conversion of GSH to GSSG as excessive ROS are produced by CI deficiency caused by *MT-ND5* mutations.

Histopathological differentiation of benign RO from malignant chRCC remains challenging, even by immunohistochemistry using multiple markers (56). Additionally, there are case reports on rare hybrid tumors (57,58), including oncocytic content, and the rare genetic disorder Brit-Hogg-Dube syndrome (59), in which RO and chRCC coexist. Microvesicle accumulation in the cytoplasm, which has been attributed to defective mitochondriogenesis, is a key histological

feature of chRCC, but has no diagnostic utility as it is also observed in RO and eosinophilic variants of ccRCC (4). Our data demonstrate that the expression profiles of ETC complex subunits can be used to distinguish these 2 tumor species. However, we want to point out that the phenotype of the 9 chRCC cases in our cohort are obviously very similar and probably belong to the classic variant, as no mitochondrial mass increase was observed by a case-by-case mitochondrial allocation analysis of the proteome data.

In summary, chRCC is characterized by downregulation of the components of the ETC and increased GSH levels, which are mainly caused by decreased mtDNA content and not CI mutation. Moreover, decreased mtDNA content in chRCC underlies the negative correlation between protein and transcript levels of nuclear DNA- but not mtDNA-encoded ETC complex subunits. These results provide insight into the molecular basis for chRCC pathology as well as markers for distinguishing this rare neoplasm from the closely related RO.

### **Acknowledgments**

This work is part of the doctoral dissertation of Y.X. Our work was supported by the Max Planck Society and the China Scholarship Council to Y.X. and the Foundation for Urologic Research (A.R. and K.J.). We are thankful to Prof. Marston Linehan, Center for Cancer Research, Bethesda, for providing the chRCC cell line UOK276.

### **References**

1. Moch H, Cubilla AL, Humphrey PA, Reuter VE, Ulbright TM. The 2016 WHO Classification of Tumours of the Urinary System and Male Genital Organs-Part A: Renal, Penile, and Testicular Tumours. *European urology* **2016**;70(1):93-105 doi 10.1016/j.eururo.2016.02.029.
2. Yusenko MV. Molecular pathology of chromophobe renal cell carcinoma: a review. *Int J Urol* **2010**;17(7):592-600 doi 10.1111/j.1442-2042.2010.02558.x.
3. Ohashi R, Schraml P, Angori S, Batavia AA, Rupp NJ, Ohe C, *et al.* Classic Chromophobe Renal Cell Carcinoma Incur a Larger Number of Chromosomal Losses Than Seen in the Eosinophilic Subtype. *Cancers (Basel)* **2019**;11(10) doi 10.3390/cancers11101492.

4. Tickoo SK, Lee MW, Eble JN, Amin M, Christopherson T, Zarbo RJ, *et al.* Ultrastructural observations on mitochondria and microvesicles in renal oncocytoma, chromophobe renal cell carcinoma, and eosinophilic variant of conventional (clear cell) renal cell carcinoma. *The American journal of surgical pathology* **2000**;24(9):1247-56 doi 10.1097/00000478-200009000-00008.
5. Akhtar M, Kardar H, Linjawi T, McClintock J, Ali MA. Chromophobe cell carcinoma of the kidney. A clinicopathologic study of 21 cases. *The American journal of surgical pathology* **1995**;19(11):1245-56 doi 10.1097/00000478-199511000-00004.
6. Latham B, Dickersin GR, Oliva E. Subtypes of chromophobe cell renal carcinoma: an ultrastructural and histochemical study of 13 cases. *The American journal of surgical pathology* **1999**;23(5):530-5 doi 10.1097/00000478-199905000-00006.
7. Haake SM, Weyandt JD, Rathmell WK. Insights into the Genetic Basis of the Renal Cell Carcinomas from The Cancer Genome Atlas. *Mol Cancer Res* **2016**;14(7):589-98 doi 10.1158/1541-7786.MCR-16-0115.
8. Brunelli M, Eble JN, Zhang S, Martignoni G, Delahunt B, Cheng L. Eosinophilic and classic chromophobe renal cell carcinomas have similar frequent losses of multiple chromosomes from among chromosomes 1, 2, 6, 10, and 17, and this pattern of genetic abnormality is not present in renal oncocytoma. *Modern pathology : an official journal of the United States and Canadian Academy of Pathology, Inc* **2005**;18(2):161-9 doi 10.1038/modpathol.3800286.
9. Casuscelli J, Weinhold N, Gundem G, Wang L, Zabor EC, Drill E, *et al.* Genomic landscape and evolution of metastatic chromophobe renal cell carcinoma. *JCI Insight* **2017**;2(12) doi 10.1172/jci.insight.92688.
10. Davis CF, Ricketts CJ, Wang M, Yang L, Cherniack AD, Shen H, *et al.* The somatic genomic landscape of chromophobe renal cell carcinoma. *Cancer cell* **2014**;26(3):319-30 doi 10.1016/j.ccr.2014.07.014.
11. Durinck S, Stawiski EW, Pavia-Jimenez A, Modrusan Z, Kapur P, Jaiswal BS, *et al.* Spectrum of diverse genomic alterations define non-clear cell renal carcinoma subtypes. *Nature genetics* **2015**;47(1):13-21 doi 10.1038/ng.3146.
12. Brauch H, Weirich G, Brieger J, Glavac D, Rodl H, Eichinger M, *et al.* VHL alterations in human clear cell renal cell carcinoma: association with advanced tumor stage and a novel hot spot mutation. *Cancer research* **2000**;60(7):1942-8.
13. Lopez-Beltran A, Scarpelli M, Montironi R, Kirkali Z. 2004 WHO classification of the renal tumors of the adults. *European urology* **2006**;49(5):798-805 doi 10.1016/j.eururo.2005.11.035.
14. Lopez-Beltran A, Carrasco JC, Cheng L, Scarpelli M, Kirkali Z, Montironi R. 2009 update on the classification of renal epithelial tumors in adults. *Int J Urol* **2009**;16(5):432-43 doi 10.1111/j.1442-2042.2009.02302.x.
15. Mayr JA, Meierhofer D, Zimmermann F, Feichtinger R, Kogler C, Ratschek M, *et al.* Loss of complex I due to mitochondrial DNA mutations in renal oncocytoma. *Clin Cancer Res* **2008**;14(8):2270-5 doi 10.1158/1078-0432.CCR-07-4131.
16. Simonnet H, Demont J, Pfeiffer K, Guenaneche L, Bouvier R, Brandt U, *et al.* Mitochondrial complex I is deficient in renal oncocytomas. *Carcinogenesis* **2003**;24(9):1461-6.
17. Gasparre G, Hervouet E, de Laplanche E, Demont J, Pennisi LF, Colombel M, *et al.* Clonal expansion of mutated mitochondrial DNA is associated with tumor formation and

- complex I deficiency in the benign renal oncocytoma. *Human molecular genetics* **2008**;17(7):986-95 doi 10.1093/hmg/ddm371.
18. Gasparre G, Romeo G, Rugolo M, Porcelli AM. Learning from oncocytic tumors: Why choose inefficient mitochondria? *Biochimica et biophysica acta* **2011**;1807(6):633-42 doi 10.1016/j.bbabi.2010.08.006.
  19. Ju YS, Alexandrov LB, Gerstung M, Martincorena I, Nik-Zainal S, Ramakrishna M, *et al.* Origins and functional consequences of somatic mitochondrial DNA mutations in human cancer. *Elife* **2014**;3 doi 10.7554/eLife.02935.
  20. Kurelac I, Iommarini L, Vatrinet R, Amato LB, De Luise M, Leone G, *et al.* Inducing cancer indolence by targeting mitochondrial Complex I is potentiated by blocking macrophage-mediated adaptive responses. *Nat Commun* **2019**;10(1):903 doi 10.1038/s41467-019-08839-1.
  21. Joshi S, Tolkunov D, Aviv H, Hakimi AA, Yao M, Hsieh JJ, *et al.* The Genomic Landscape of Renal Oncocytoma Identifies a Metabolic Barrier to Tumorigenesis. *Cell Rep* **2015**;13(9):1895-908 doi 10.1016/j.celrep.2015.10.059.
  22. Davis CF, Ricketts CJ, Wang M, Yang L, Cherniack AD, Shen H, *et al.* The somatic genomic landscape of chromophobe renal cell carcinoma. *Cancer cell* **2014**;26(3):319-30 doi 10.1016/j.ccr.2014.07.014.
  23. Ricketts CJ, De Cubas AA, Fan H, Smith CC, Lang M, Reznik E, *et al.* The Cancer Genome Atlas Comprehensive Molecular Characterization of Renal Cell Carcinoma. *Cell Rep* **2018**;23(1):313-26 e5 doi 10.1016/j.celrep.2018.03.075.
  24. Larman TC, DePalma SR, Hadjipanayis AG, Cancer Genome Atlas Research N, Protopopov A, Zhang J, *et al.* Spectrum of somatic mitochondrial mutations in five cancers. *Proc Natl Acad Sci U S A* **2012**;109(35):14087-91 doi 10.1073/pnas.1211502109.
  25. Kurschner G, Zhang Q, Clima R, Xiao Y, Busch JF, Kilic E, *et al.* Renal oncocytoma characterized by the defective complex I of the respiratory chain boosts the synthesis of the ROS scavenger glutathione. *Oncotarget* **2017**;8(62):105882-904 doi 10.18632/oncotarget.22413.
  26. Gopal RK, Calvo SE, Shih AR, Chaves FL, McGuone D, Mick E, *et al.* Early loss of mitochondrial complex I and rewiring of glutathione metabolism in renal oncocytoma. *Proceedings of the National Academy of Sciences of the United States of America* **2018**;115(27):E6283-E90 doi 10.1073/pnas.1711888115.
  27. Priolo C, Khabibullin D, Reznik E, Filippakis H, Ogorek B, Kavanagh TR, *et al.* Impairment of gamma-glutamyl transferase 1 activity in the metabolic pathogenesis of chromophobe renal cell carcinoma. *Proceedings of the National Academy of Sciences of the United States of America* **2018**;115(27):E6274-E82 doi 10.1073/pnas.1710849115.
  28. Xiao Y, Clima R, Busch JF, Rabien A, Kilic E, Villegas S, *et al.* Metabolic reprogramming and elevation of glutathione in chromophobe renal cell carcinomas. *bioRxiv* **2019**:649046 doi 10.1101/649046.
  29. Jaakkola P, Mole DR, Tian YM, Wilson MI, Gielbert J, Gaskell SJ, *et al.* Targeting of HIF-alpha to the von Hippel-Lindau ubiquitylation complex by O2-regulated prolyl hydroxylation. *Science* **2001**;292(5516):468-72 doi 10.1126/science.1059796.
  30. Xiao Y, Meierhofer D. Glutathione Metabolism in Renal Cell Carcinoma Progression and Implications for Therapies. *Int J Mol Sci* **2019**;20(15) doi 10.3390/ijms20153672.

31. Kulak NA, Pichler G, Paron I, Nagaraj N, Mann M. Minimal, encapsulated proteomic-sample processing applied to copy-number estimation in eukaryotic cells. *Nature methods* **2014**;11(3):319-24 doi 10.1038/nmeth.2834.
32. Cox J, Mann M. MaxQuant enables high peptide identification rates, individualized p.p.b.-range mass accuracies and proteome-wide protein quantification. *Nature biotechnology* **2008**;26(12):1367-72 doi 10.1038/nbt.1511.
33. Gielisch I, Meierhofer D. Metabolome and proteome profiling of complex I deficiency induced by rotenone. *J Proteome Res* **2015**;14(1):224-35 doi 10.1021/pr500894v.
34. Calabrese C, Simone D, Diroma MA, Santorsola M, Gutta C, Gasparre G, *et al.* MToolBox: a highly automated pipeline for heteroplasmy annotation and prioritization analysis of human mitochondrial variants in high-throughput sequencing. *Bioinformatics* **2014**;30(21):3115-7 doi 10.1093/bioinformatics/btu483.
35. Talevich E, Shain AH, Botton T, Bastian BC. CNVkit: Genome-Wide Copy Number Detection and Visualization from Targeted DNA Sequencing. *PLoS Comput Biol* **2016**;12(4):e1004873 doi 10.1371/journal.pcbi.1004873.
36. Goldman M, Craft B, Hastie M, Repečka K, Kamath A, McDade F, *et al.* The UCSC Xena Platform for cancer genomics data visualization and interpretation. *bioRxiv* **2019**:326470 doi 10.1101/326470.
37. Li B, Dewey CN. RSEM: accurate transcript quantification from RNA-Seq data with or without a reference genome. *BMC bioinformatics* **2011**;12:323 doi 10.1186/1471-2105-12-323.
38. Yang Y, Vocke CD, Ricketts CJ, Wei D, Padilla-Nash HM, Lang M, *et al.* Genomic and metabolic characterization of a chromophobe renal cell carcinoma cell line model (UOK276). *Genes Chromosomes Cancer* **2017**;56(10):719-29 doi 10.1002/gcc.22476.
39. Tyanova S, Temu T, Sinitcyn P, Carlson A, Hein MY, Geiger T, *et al.* The Perseus computational platform for comprehensive analysis of (prote)omics data. *Nature methods* **2016**;13(9):731-40 doi 10.1038/nmeth.3901.
40. Subramanian A, Tamayo P, Mootha VK, Mukherjee S, Ebert BL, Gillette MA, *et al.* Gene set enrichment analysis: a knowledge-based approach for interpreting genome-wide expression profiles. *Proceedings of the National Academy of Sciences of the United States of America* **2005**;102(43):15545-50 doi 10.1073/pnas.0506580102.
41. Vizcaino JA, Cote RG, Csordas A, Dianes JA, Fabregat A, Foster JM, *et al.* The PRoteomics IDentifications (PRIDE) database and associated tools: status in 2013. *Nucleic acids research* **2013**;41(Database issue):D1063-9 doi 10.1093/nar/gks1262.
42. Li N, Ragheb K, Lawler G, Sturgis J, Rajwa B, Melendez JA, *et al.* Mitochondrial complex I inhibitor rotenone induces apoptosis through enhancing mitochondrial reactive oxygen species production. *The Journal of biological chemistry* **2003**;278(10):8516-25 doi 10.1074/jbc.M210432200.
43. Chen Q, Vazquez EJ, Moghaddas S, Hoppel CL, Lesnefsky EJ. Production of reactive oxygen species by mitochondria: central role of complex III. *The Journal of biological chemistry* **2003**;278(38):36027-31 doi 10.1074/jbc.M304854200.
44. Asensi M, Sastre J, Pallardo FV, Lloret A, Lehner M, Garcia-de-la Asuncion J, *et al.* [23] Ratio of reduced to oxidized glutathione as indicator of oxidative stress status and DNA damage. *Methods in Enzymology*. Volume 299: Academic Press; 1999. p 267-76.

45. Goldstein A, Falk MJ. Mitochondrial DNA Deletion Syndromes. In: Adam MP, Ardinger HH, Pagon RA, Wallace SE, Bean LJH, Stephens K, *et al.*, editors. GeneReviews((R)). Seattle (WA)1993.
46. Yusoff AAM, Abdullah WSW, Khair S, Radzak SMA. A comprehensive overview of mitochondrial DNA 4977-bp deletion in cancer studies. *Oncol Rev* **2019**;13(1):409 doi 10.4081/oncol.2019.409.
47. Aretz I, Hardt C, Wittig I, Meierhofer D. An Impaired Respiratory Electron Chain Triggers Down-regulation of the Energy Metabolism and De-ubiquitination of Solute Carrier Amino Acid Transporters. *Mol Cell Proteomics* **2016**;15(5):1526-38 doi 10.1074/mcp.M115.053181.
48. Meierhofer D, Mayr JA, Foetschl U, Berger A, Fink K, Schmeller N, *et al.* Decrease of mitochondrial DNA content and energy metabolism in renal cell carcinoma. *Carcinogenesis* **2004**;25(6):1005-10 doi 10.1093/carcin/bgh104.
49. King MP, Attardi G. [27] Isolation of human cell lines lacking mitochondrial DNA. *Methods in Enzymology*. Volume 264: Academic Press; 1996. p 304-13.
50. Thoenes W, Storkel S, Rumpelt HJ. Human chromophobe cell renal carcinoma. *Virchows Arch B Cell Pathol Incl Mol Pathol* **1985**;48(3):207-17.
51. Al Ahmad A, Paffrath V, Clima R, Busch JF, Rabien A, Kilic E, *et al.* Papillary Renal Cell Carcinomas Rewire Glutathione Metabolism and Are Deficient in Both Anabolic Glucose Synthesis and Oxidative Phosphorylation. *Cancers (Basel)* **2019**;11(9) doi 10.3390/cancers11091298.
52. Wettersten HI, Hakimi AA, Morin D, Bianchi C, Johnstone ME, Donohoe DR, *et al.* Grade-Dependent Metabolic Reprogramming in Kidney Cancer Revealed by Combined Proteomics and Metabolomics Analysis. *Cancer research* **2015**;75(12):2541-52 doi 10.1158/0008-5472.CAN-14-1703.
53. Hakimi AA, Reznik E, Lee CH, Creighton CJ, Brannon AR, Luna A, *et al.* An Integrated Metabolic Atlas of Clear Cell Renal Cell Carcinoma. *Cancer cell* **2016**;29(1):104-16 doi 10.1016/j.ccell.2015.12.004.
54. Circu ML, Aw TY. Glutathione and apoptosis. *Free Radic Res* **2008**;42(8):689-706 doi 10.1080/10715760802317663.
55. Grandhi S, Bosworth C, Maddox W, Sensiba C, Akhavanfard S, Ni Y, *et al.* Heteroplasmic shifts in tumor mitochondrial genomes reveal tissue-specific signals of relaxed and positive selection. *Human molecular genetics* **2017**;26(15):2912-22 doi 10.1093/hmg/ddx172.
56. Ng KL, Morais C, Bernard A, Saunders N, Samaratunga H, Gobe G, *et al.* A systematic review and meta-analysis of immunohistochemical biomarkers that differentiate chromophobe renal cell carcinoma from renal oncocytoma. *J Clin Pathol* **2016**;69(8):661-71 doi 10.1136/jclinpath-2015-203585.
57. Noguchi S, Nagashima Y, Shuin T, Kubota Y, Kitamura H, Yao M, *et al.* Renal oncocytoma containing "chromophobe" cells. *Int J Urol* **1995**;2(4):279-80.
58. Pote N, Vieillefond A, Couturier J, Arrufat S, Metzger I, Delongchamps NB, *et al.* Hybrid oncocytic/chromophobe renal cell tumours do not display genomic features of chromophobe renal cell carcinomas. *Virchows Arch* **2013**;462(6):633-8 doi 10.1007/s00428-013-1422-4.

59. Vera-Badillo FE, Conde E, Duran I. Chromophobe renal cell carcinoma: a review of an uncommon entity. *Int J Urol* **2012**;19(10):894-900 doi 10.1111/j.1442-2042.2012.03079.x.

## Figure legends

**Figure 1. Differential regulation of ETC complexes in chRCC and RO.** (A, B) Comparison of protein abundance ratios ( $\log_2$ ) of ETC complex subunits between chRCC (A) and RO (B) tissue vs healthy kidney tissue samples. The 5 ETC complexes—including all quantified subunits and assembly factors—and corresponding  $\log_2$  fold changes are shown. The color gradient reflects low (blue) or high (red) abundance of the protein in the tumor. The abundance of CI subunits was decreased in chRCC and RO, whereas the levels of all other ETC complexes were increased in RO while generally showing low abundance in chRCC. Assembly factors (bold type) that are not part of the final complex were upregulated in both tumor types. \*FDR  $\leq$  0.05. (C, D) Comparison of the density of mitochondrial and non-mitochondrial proteins vs  $\log_2$  fold change of proteins between RO and healthy kidney tissue (C) and between chRCC and healthy kidney tissue (D). Mitochondrial proteins are shown in red (Human Mito Carta, 1158 entries) and non-mitochondrial proteins are shown in blue.

**Figure 2. Comparative analysis of RNA and protein abundance between chRCC and healthy kidney tissue.** (A, B) GSEA revealed that ETC complex components were downregulated at the protein level (this study) (A) and upregulated at the transcript level (TCGA data; B). (C) Global transcript versus protein levels are shown as blue dots, proteins localized to mitochondria as red triangles, and specific factors involved in the ETC as green squares, indicating the discrepancy between transcript and protein levels exclusively for the ETC. RNA data were retrieved from TCGA. (D–H) Comparison of enzyme activity (nmol/min/mg protein, n=9) of ETC complexes between chRCC and healthy kidney tissue, including CI (D), CII (E), CIII (F), CIV (G), and CV (H). \* $P < 0.05$ , \*\* $P < 0.01$ , \*\*\* $P < 0.001$  (paired t test); n.s., not significant.

**Figure 3. GSH levels are elevated in chRCC.** (A–C) Relative abundance of metabolites involved in GSH metabolism is shown for chRCC and healthy kidney tissue samples. Levels of

reduced GSH (A), oxidized GSH (B), and gamma-glutamylcysteine (C) are shown. (D) GSH/GSSG ratio calculated based on relative signal intensity. (E) Heatmap of quantified proteins involved in GSH metabolism in chRCC. The color gradient represents a low (blue) or high (red)  $\log_2$  fold change in chRCC vs normal kidney tissue. \*\* $P < 0.01$ , \*\*\* $P < 0.001$  (2-tailed Student's t test). A.U., arbitrary units.

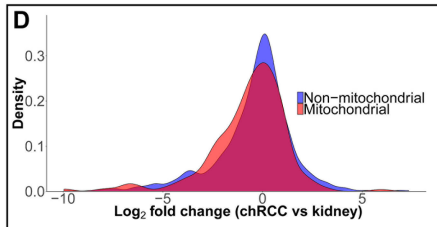
**Figure 4. Identified somatic mtDNA mutations and mtDNA copy number in chRCC.** (A) Somatic mtDNA mutations with a high disease score ( $>0.7$ ) were detected in 5 tumors; only the *MT-ND5* mutation in Case 4 had a significant heteroplasmy rate. (B) Decreased mtDNA read depth indicating a lower mtDNA copy number in chRCC compared to normal kidney tissue (n=9). \* $P < 0.05$  (paired t test).

**Figure 5. Correlation between mtDNA content, ETC protein and transcript levels, and GSH level.** (A) mtDNA content over time in UOK276 chRCC cells treated with ethidium bromide (EtBr) (100 ng/ml). The cells were used for all subsequent analyses (n = 3). (B) Western blot analysis of mtDNA- and nuclear DNA-encoded ETC complex subunits MT-ND5, NDUFS1, SDHB, and UQCRC2, showing a time-dependent decrease in abundance. (C) Increased GSH level in chRCC cells and an inverse correlation with mtDNA content over time. (D) Transcript levels of nuclear DNA-encoded NDUFS1, SDHB, and UQCRC2 initially decreased but then increased. The mtDNA-encoded MT-ND5 transcript decreased in the first 2 days in parallel with mtDNA content, but did not increase thereafter. The error bar indicates the standard deviation. \* $P < 0.05$  (2-tailed Student's t-test). n.s., not significant.

# Figure 1

A

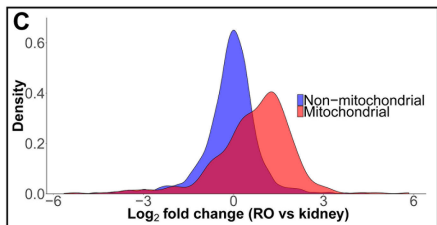
|              |              |
|--------------|--------------|
| NDUFB6       | 0.02         |
| NDUFA6       | -0.17        |
| NDUFAB1      | -0.23        |
| NDUFS5       | -0.40        |
| NDUFB11      | -0.58        |
| <b>NDUF2</b> | <b>-0.70</b> |
| <b>ACAD9</b> | <b>-0.72</b> |
| NDUFA5       | -0.83        |
| NDUFB10      | -0.97*       |
| NDUFA13      | -1.01*       |
| NDUFA11      | -1.07*       |
| NDUFA8       | -1.29        |
| NDUFB5       | -1.67*       |
| NDUFB7       | -1.77*       |
| NDUFA9       | -1.96*       |
| NDUFC2       | -1.98*       |
| NDUFB1       | -2.10*       |
| NDUFB4       | -2.34*       |
| NDUFB3       | -2.35*       |
| NDUFA3       | -2.55*       |
| NDUFS6       | -2.56*       |
| NDUFB9       | -2.69*       |
| NDUFA10      | -2.75*       |
| NDUFA12      | -2.81*       |
| NDUFB8       | -2.84*       |
| NDUFA7       | -2.87*       |
| NDUFS4       | -2.95*       |
| NDUFB3       | -3.35*       |
| NDUFA2       | -3.54*       |
| NDUFB4       | -2.34*       |
| <b>NDUF4</b> | <b>2.48*</b> |
| <b>NDUF3</b> | <b>2.05*</b> |
| NUBPL        | 0.11         |
| NDUFS3       | -0.68*       |
| NDUFS2       | -0.76*       |
| MT-ND5       | -1.66*       |
| MT-ND1       | -1.76*       |
| NDUFV2       | -1.93*       |
| NDUFS1       | -1.95*       |
| NDUFV1       | -3.23*       |



|               |               |
|---------------|---------------|
| COX7A1        | 1.05          |
| <b>SCO2</b>   | <b>0.26</b>   |
| <b>COX17</b>  | <b>0.20</b>   |
| COX5A         | -0.14         |
| COX4I1        | -0.26         |
| COX6B1        | -0.36         |
| COA6          | <b>-0.51</b>  |
| COX5B         | -0.64*        |
| <b>COA4</b>   | <b>-1.01*</b> |
| MT-CO2        | -1.22*        |
| MT-CO3        | -1.28*        |
| MT-CO1        | -1.51*        |
| COX6C         | -2.32*        |
| COX7A2        | -2.40*        |
| UQCRH         | 0.93          |
| CYC1          | 0.66*         |
| UQCR10        | 0.11          |
| UQCRFS1       | 0.00          |
| UQCRC2        | -0.16         |
| UQCRB         | -0.27         |
| UQCRQ         | -0.28         |
| <b>UQCRC1</b> | <b>-0.40</b>  |
| MT-CYB        | -1.22         |
| SDHA          | -0.65*        |
| SDHB          | -0.78*        |
| SDHC          | -1.35*        |
| SDHD          | -1.40         |
| <b>ATPAF1</b> | <b>1.10</b>   |
| ATP5C1        | 0.10          |
| ATP5A1        | 0.07          |
| ATP5D         | 0.01          |
| ATP5B         | -0.07         |
| ATP5O         | -0.20         |
| ATP5L         | -0.43         |
| ATP5L         | -0.54*        |
| ATP5J2        | -0.68*        |
| ATP5F1        | -0.78*        |
| ATP5H         | -0.86*        |
| ATP5J         | -1.13         |
| <b>ATPIF1</b> | <b>-2.38*</b> |

B

| Complex I    | Complex II | Complex III        | Complex IV         | Complex V          |
|--------------|------------|--------------------|--------------------|--------------------|
| NDUFA7       | SDHB 0.66  | UQCRFS1 0.44       | <b>COA4</b> -0.09  | <b>ATPAF1</b> 0.08 |
| NDUFB9       | SDHA 1.32  | UQCRQ 1.22         | <b>COA7</b> 0.69   | ATP5C1 0.24        |
| NDUFS6       |            | CYC1 1.39*         | COX7A2 0.99        | ATP5L 0.46         |
| NDUFB7       |            | UQCRC1 1.59        | <b>COX20</b> 1.03  | ATP5F1 0.73        |
| NDUFS1       |            | UQCRC2 1.59        | MT-CO2 1.14        | ATP5B 0.86         |
| NDUFA10      |            | UQCRH 1.60*        | <b>COA6</b> 1.31   | ATP5O 0.92         |
| NDUFS5       |            | UQCRB 2.11         | COX4I1 1.34        | ATP5A1 0.94        |
| NDUFV1       |            | <b>UQCC2</b> 2.67* | COX7C 1.38         | ATP5H 1.13         |
| NDUFA2       |            |                    | COX5B 1.43         | ATP5J 1.48         |
| NDUFB1       |            |                    | COX5A 1.47         | ATP5I 1.55         |
| NDUFV2       |            |                    | COX6C 1.50         | ATP5D 1.57         |
| NDUFA13      |            |                    | <b>SCO1</b> 1.61   | ATP5J2 2.02        |
| NDUFS8       |            |                    | COX6B1 1.76*       | <b>ATP5E</b> 3.13  |
| NDUFS2       |            |                    | COX6A1 2.14        |                    |
| NDUFS3       |            |                    | <b>COX17</b> 2.27* |                    |
| NDUFA6       |            |                    |                    |                    |
| NDUFS7       |            |                    |                    |                    |
| NDUFB6       |            |                    |                    |                    |
| NDUFA8       |            |                    |                    |                    |
| NDUFB10      |            |                    |                    |                    |
| NDUFAB1      |            |                    |                    |                    |
| NDUFA5       |            |                    |                    |                    |
| <b>NDUF2</b> |            |                    |                    |                    |
| <b>NDUF4</b> |            |                    |                    |                    |



Font in bold: Assembly factor

# Figure 2

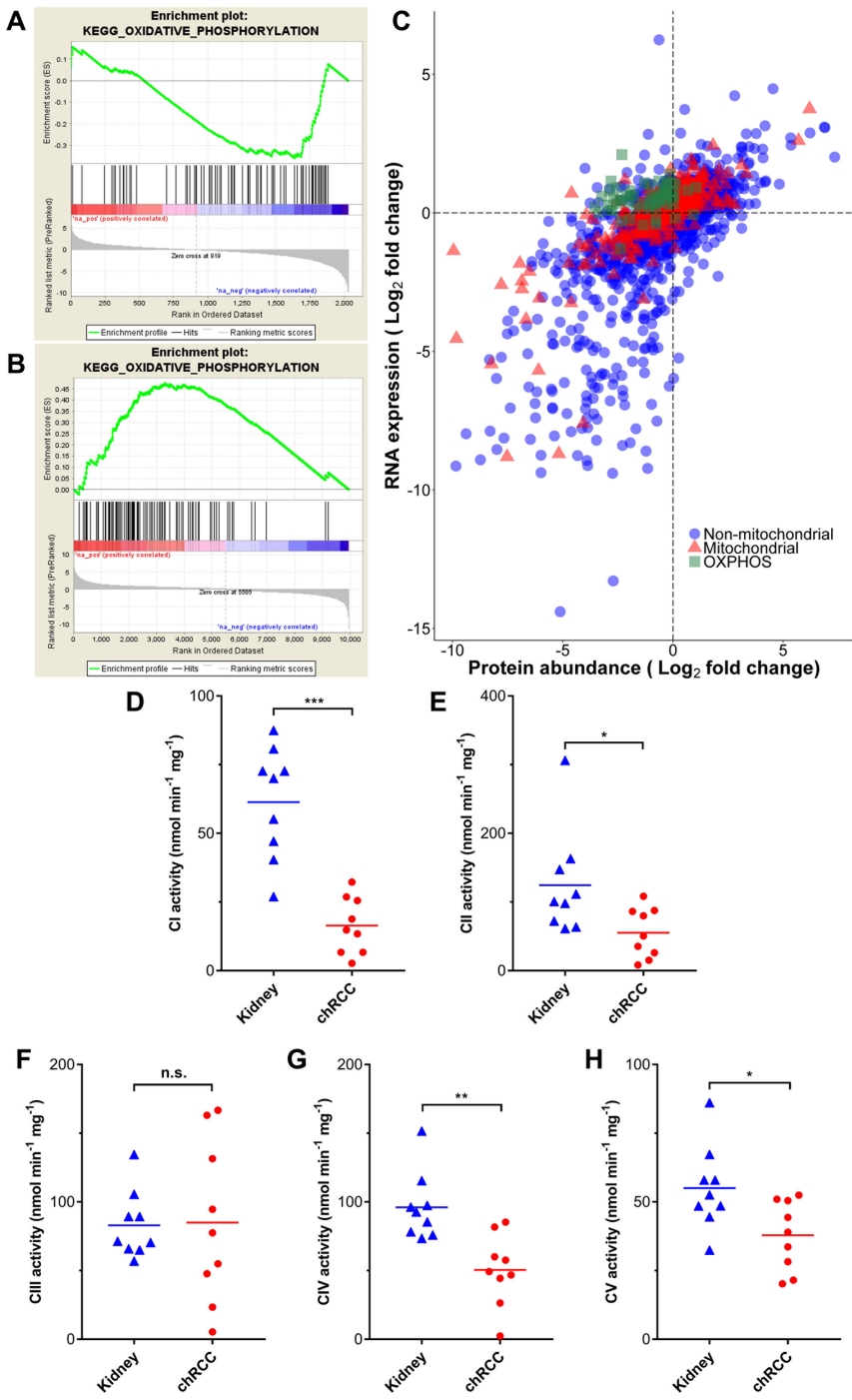


# Figure 3

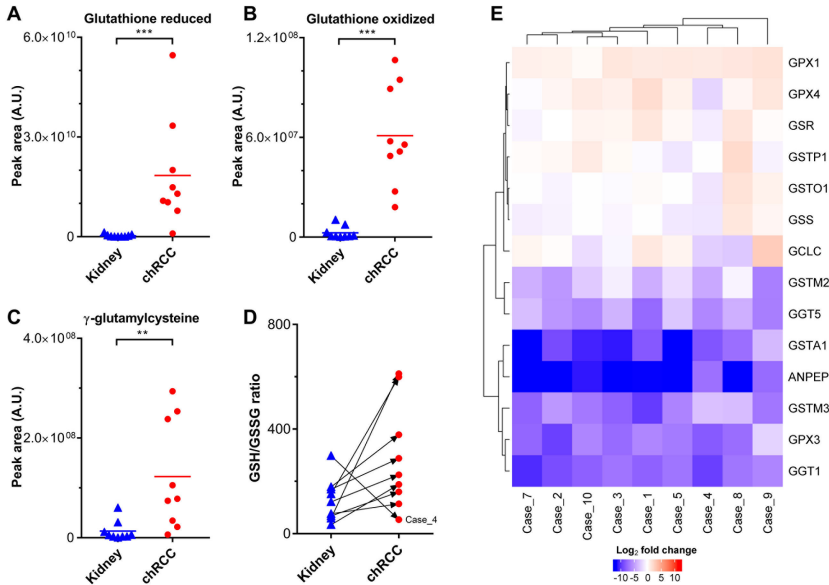




# Figure 5

